Photocatalytic decoloration of three commercial dyes in aqueous phase and industrial effluents using TiO$_2$ nanoparticles

Hiral Soni[a,*], J.I. Nirmal Kumar[a], Khushal Patel[b], Rita N. Kumar[c]

[a]Department of Environment Science and Technology (DEST), Institute of Science and Technology for Advanced Studies and Research (ISTAR), Vallabh Vidyanagar 388120, Gujarat, India, Tel. +91 9978033036; email: hiralsoni@ymail.com (H. Soni), Tel. +91 9825968242; email: nirmalkji@gmail.com (J.I.N. Kumar)
[b]Department of Bioscience, Ashok and Rita Patel Institute of Integrated Study and Research in Biotechnology and Allied Sciences, New Vallabh Vidyanagar 3888121, Gujarat, India, Tel. +91 9978365630; email: khushalbiotechstudent@yahoo.co.in
[c]Department of Bioscience & Environment Science, N.V. Patel College of Pure and Applied Sciences, Vallabh Vidyanagar 388120, Gujarat, India, Tel. +91 9825924687; email: ritankumar@yahoo.co.in

ABSTRACT

TiO$_2$ sol was synthesized under mild conditions (25 ± 1°C and ambient pressure) by hydrolysis of titanium isopropoxide in aqueous solution and subsequent reflux to enhance crystallization. The material was characterized by X-ray diffraction, transmission electron microscopy, and Fourier transform infrared. The synthesized sample presented a pure phase anatase with nanometric particle size. The photodegradation of reactive dyes (malachite green, methylene blue, and rhodamine B) and industrial effluents was elucidated in aqueous suspension containing titania nanoparticles under UV irradiation. Also, the effect of pH in nanoparticle synthesis and role of catalyst dose and dye concentration were evaluated. The experimental result showed that particles synthesized by sol–gel method are of 20–40 nm anatase form with cuboidal structure and OH$^-$ as a major functional group. These particles showed efficiency to degrade dyes up to 98% and industry (paint and textile) effluents can be decolorized in the TiO$_2$/UV system.

Keywords: Methylene Blue; Malachite Green; Rhodamine B; Industrial effluents; TiO$_2$ adsorbent; Photocatalysis

1. Introduction

Now-a-days, most colorants have the purpose to satisfy the esthetical needs of the environment and thus, thousands of dyes and pigments are produced in industrial scales [1]. Textile industry has shown a significant increase in the use of synthetic complex organic dyes as coloring material [2]. Synthetic dyestuffs, a group of organic pollutants, are used extensively in textile, paper, printing industries, and dye houses. It is reported that there are over 100,000 commercially available dyes with a production of over 7×10^5 metric tonnes per year [3,4]. Estimates indicate that approximately 10–20% of the synthetic textile dyes used are lost in waste streams during manufacturing or processing operations [5,6]. Even at low concentrations, textile wastewater is intensely colored. It poses genotoxic and carcinogenic properties and affects the immune system and reproductive system.

*Corresponding author.

Reactive dyes have been identified as the most environmental problematic compounds in textile dye effluents [7,8]. Most of the dyes and poisonous metals used in the textile industries are stable to light and are non-biodegradable [9]. In order to reduce the risk of environmental pollution from such waste, it is necessary to treat them before discharging into the environment. There are various methods for removal of organic and inorganic compounds from the wastewater such as filtration, electrolysis, precipitation, ion-exchange and adsorption processes [10,11]. Most of these methods require high capital and recurring expenditure and consequently they are not suitable for small-scale industries [12]. Among all the above-mentioned methods, photocatalysis is highly effective and cheap process than the other methods [13]. Besides, photocatalytic detoxification is a process where a semiconductor upon adsorption of a photon acts as a catalyst in producing reactive radicals, mainly hydroxyl radicals, which in turn can oxidize organic compounds and totally neutralize and/or completely destroy the organic and inorganic compounds in the water instead of simply removing or displacing [14].

In this paper, an attempt has been made on the synthesis and characterization of TiO_2 nanoparticles and removal of the most commonly used coloring dyes such as malachite green, methylene blue, rhodamine B, and industry effluents (paint and textile industry effluents) by anatase TiO_2 nanoadsorbent. These dyes are used for present study, because they are the brightest class of soluble dyes used in textile and color industry [15,16]. Moreover, the influence of pH on nanoparticle synthesis, role of dye concentration, and catalyst dose in photocatalytic activity was evaluated.

2. Materials and methods

2.1. Materials

Reactive dyes were purchased from Merck India and their properties are mentioned in Table 1 [16–19]. Titanium tetraisopropoxide (97%) and acetic acid (99.7%) were purchased from Hi-media, while chemicals of analytical reagent grade were used without further purification. Double-distilled water was used as the solvent for all the studies and Ultraviolet (UV-C) with two 15-W lamps (Philips Model) was used as the source of UV radiation (with constant intensity = 2.8 mW/cm^2).

2.2. Catalyst preparation

TiO_2 nanoparticles were synthesized following a procedure reported elsewhere [20]. The synthesis was carried out at a high degree of super saturation in order to achieve a nucleation rate much greater than the growth rate. The samples were prepared by a modified sol–gel route [21]. Twelve milliliter titanium isopropoxide was added to 23 mL of acetic acid with continuous stirring. After that, 72 mL water was added to the mixture drop by drop with vigorous stirring. pH was adjusted to 1, 3, 6, and 9 by dilute HNO_3 for acidic condition and NaOH for basic condition. The solution was stirred for 6 h until a clear transparent sol was achieved; it was dried at 100℃, and after that it was calcined at 600℃ for 2 h at a ramp rate of 5℃/min. Then, particles were characterized for their shape, size, and identification of functional groups. The photocatalytic activities of the materials were studied by examining the degradation reaction.
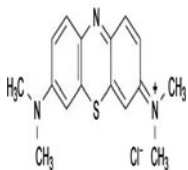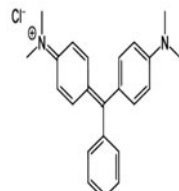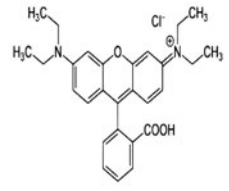
2.3. Physico-chemical catalytic characterization

The crystallinity was determined by Powder XRD (Phillips X'pert MPD system, Holland) using Cu–Kα radiation ($\lambda = 1.5405$ Å) in a 2y range of 5–601 at a scan speed of 0.11 s^{-1}, maintaining applied voltage at 40 kV and current at 40 mA. About 0.5 g of the dried particles was deposited as a randomly oriented powder onto a Plexiglas sample container, and the XRD patterns were recorded between 20° and 80° angles. XRD patterns were compared with the standard anatase diffractograms [22]. The shape and size of the particles were obtained through transmission electron microscope (TEM) using a model Philips Tecnai 20, Holland with an accelerating voltage of 100 kV. For TEM measurements, the samples were placed on carbon-coated copper grids. This sample was prepared from much diluted dispersions of the particles in 2-propanol. The chemical composition of the synthesized material was evaluated using Fourier transform infrared (FTIR) spectrophotometer (SPECTRUM GX, Perkin-Elmer). The spectrum is recorded in the range of wave number 400–4,000 cm^{-1} [23].

2.4. Photocatalytic experiment

Batch experiments were carried out using a series of Erlenmeyer flask of 50 mL capacity covered with aluminum foil to prevent the introduction of any foreign particle contamination. The effects of concentration of dye solution and dose of catalyst were studied. Isotherms were run by taking selected different concentrations (10, 20, 30, and 40 ppm) of methylene blue, malachite green, and rhodamine B. Dye-containing flasks were stirred in dark for half an hour. For kinetic studies, the batch technique was used due to its

Table 1
Chemical structure and properties of methylene blue, malachite green, and rhodamine B

Dye	Methylene Blue	Malachite Green	Rhodamine B
Structure			
λ_{max}	660 nm	610 nm	550 nm
M_w	319.86	464.91	479.02
IUPAC name	3,7-bis (Dimethylamino)- phenothiazin-5-ium chloride	4-{[4-(dimethylamino)phenyl](phenyl) methylidene}-N,N-dimethylcyclohexa-2,5- dien-1-iminium chloride	[9-(2-carboxyphenyl)-6-diethylamino- 3-xanthenylidene]-diethylammonium chloride
C.I. number		C.I. 52015	C.I. 52015
C.I. 45170			

simplicity. From flasks, defined volumes of methylene blue, malachite green, and rhodamine B were taken in test tubes to which known different amount of the catalyst was added to each tube. Catalyst-containing tubes were placed directly on the surface of UV-radiation lamp. Four 15 W low-pressure mercury UV tubes (Spectronics) emitting near UV radiation with a peak at 365 nm were used (Fig. 1). The photocatalytic oxidation process started when UV radiation reached the TiO_2 photocatalyst. Then, tubes were allowed to agitate occasionally by gentle stirring. At given time intervals, various parameters like temperature and pH were measured. Then, samples were centrifuged and the supernatants were analyzed for methylene blue, malachite green, and rhodamine B by a UV–vis spectrophotometer. The residual dye concentration in each solution was measured spectrophotometrically at the corresponding λ_{max} (665, 615, and 555 nm for methylene blue, malachite green, and rhodamine B, respectively). Blank sample tube-containing dye without nanocatalyst was also placed on UV irradiation. This shows that during UV irradiation, decolorization of dyes only takes place in the presence of a photocatalyst [24]. In the photodegradation experiments, the extent of removal of the dye in terms of the values of percentage removal has been calculated using the following relationship:

$$\text{Percentage removal } (\%R) = 100 \times (C_i - C_f)/C_f$$

where C_i, initial concentration of dye (ppm); C_f, final concentration of dye (ppm) at given time.
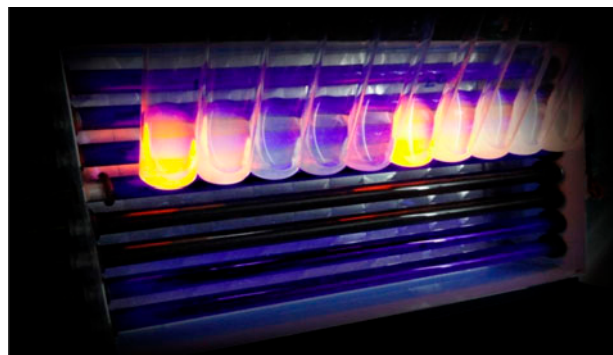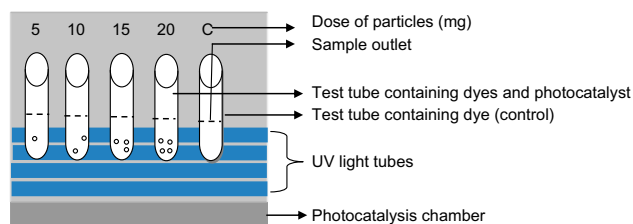

Fig. 1. Schematic diagram and photography of photocatalytic experiment.

Similarly, photocatalytic experiment was carried out with paint industry effluent and textile industry effluent. Samples were collected from the source point outlet of finishing unit of industry. Some physicochemical parameters of the effluent like pH, COD, ions-PO_4, SO_4, NO_3 and hardness were measured.

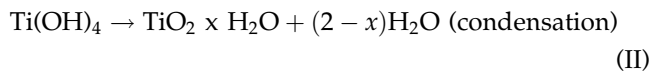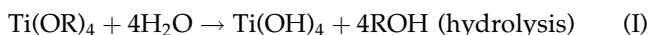Distinct amount (10, 20, and 30%) of crude effluent sample was taken and high dose of particles were

added and UV treatment was applied. Percentage degradation was calculated. Photocatalysis experiment was repeated three times.

3. Results and discussion

3.1. X-ray diffraction

Fig. 2 shows the X-ray diffraction (XRD) patterns of the powder samples prepared in initial solution with different pH. From these patterns, it is easy to see distinct peaks at 25.3°. It is also noticed that pH affects particles size and degree of crystallinity. A trace of rutile was found in sample prepared at pH 9 at 30.21° with high peaks of impurities. In this case, it is found that lower acidity will favor anatase formation [25,26].

The preparation of the TiO$_2$ colloids in the nano range can be effectively conducted through the hydrolysis and condensation of titanium alkoxides in aqueous media. In the presence of water, alkoxides are hydrolyzed and subsequently polymerized to form a three-dimensional oxide network. These reactions can be schematically represented as follows:

$$Ti(OR)_4 + 4H_2O \rightarrow Ti(OH)_4 + 4ROH \text{ (hydrolysis)} \quad (I)$$

$$Ti(OH)_4 \rightarrow TiO_2 \text{ x } H_2O + (2 - x)H_2O \text{ (condensation)} \quad (II)$$

where R is ethyl, *i*-propyl, *n*-butyl, etc. [27]. It is well known that the tetravalent cations are too much acidic so that the nucleation of stable hydroxide Ti(OH)$_4$ cannot occur. Water molecules formed according to reaction (II) always bear a positive partial charge [28]. Therefore, oxolation and olation can proceed simultaneously during nucleation and growth leading to the formation of amorphous hydrous oxide (TiO$_2$·nH$_2$O), where the number n of water molecules depends on experimental conditions. Depending on the experimental procedure, the precipitation of TiO$_2$ lead to rutile or anatase phases [29]. The formation of such structures from aqueous molecular precursors can be described as follows: when deoxolation (O Ti–OH$_2$ → HO–Ti–Ti–OH) does not occur during nucleation, olation leads to a linear growth along one of the two equivalent directions in the equatorial plane of [Ti$_2$O$_2$(OH)$_4$(OH2)$_4$]0 dimers. Then, oxolation between the resulting TiO(OH)$_2$(OH)$_2$ linear chains after an internal proton transfer leads to corner-sharing octahedral chains (Ti$_3$O bridges) characteristics of the rutile structure. The formation of rutile may then be associated to the metastability of apical Ti O bonds within monomers or dimers. Now, if deoxolation occurs prior
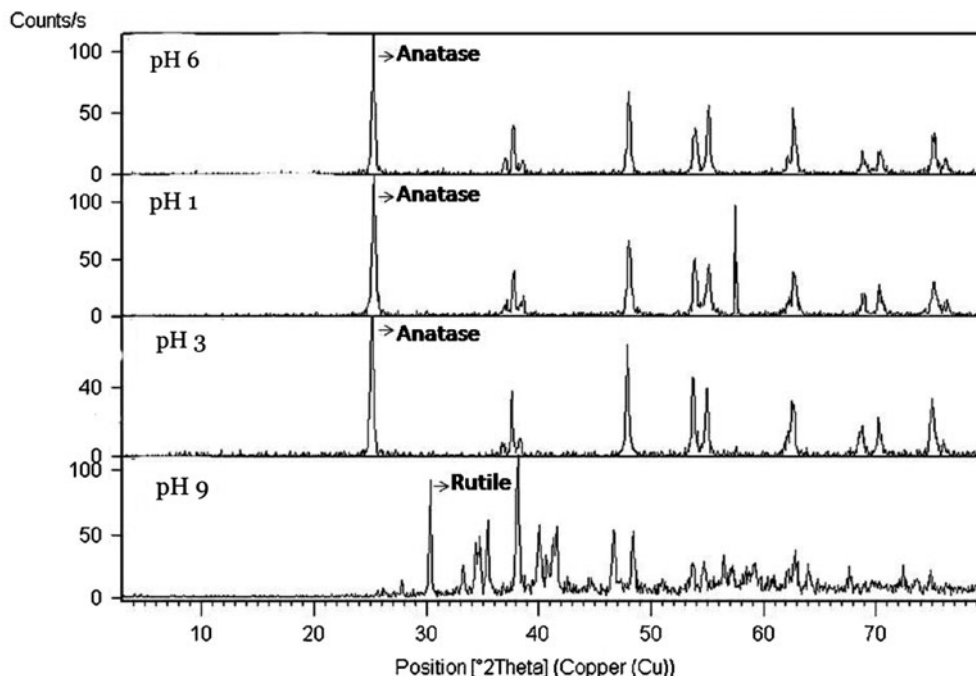

Fig. 2. XRD patterns of nanocrystalline titania samples prepared by sol–gel method with various pH conditions such as (a) pH 6, (b) pH 1, (c) pH 3, and (d) pH 9.

Table 2
Crystallite size of sample prepared via sol–gel method

pH	Crystallite size (nm)
1	23
3	23
6	24
9	47

to olation, condensation can proceed along apical direction leading to skewed chains typical of the anatase structure. Controlling the stage of deoxolation prior to olation can be obtained by adjusting the pH and initial water concentration. This control leads to precipitation of anatase nanopowder TiO_2 in the experimental procedure.

The crystallite size was determined by Scherrer equation and summarized in Table 2. It was found that the crystallite size varies from 23 to 47 nm.

When the pH level of the solution is lower than 6 i.e. more acidic, a white suspension of rough precipitant is formed immediately after hydrolysis reaction. However, when the pH level is above 6, homogeneous suspension of fine particles is formed. Table 2 shows that smaller crystals from homogeneous suspension have been obtained from the hydrolysis of TTIP in the

slight acidic solution (pH 6). So, further characterization followed by photocatalysis was performed using particles prepared at pH 6.

3.2. Functional group analysis of TiO_2 nanoparticles

FTIR spectrum of as-synthesized anatase TiO_2 nanoparticles is shown in Fig. 3. It was observed that the strong band in the range of 700–500 cm^{-1} is associated with the characteristic vibrational modes of TiO_2. This confirms that the TiO_2 phase has been formed. The absorption in the range from 3,500 to 2,500 cm^{-1} may be related to the presence of O–H stretching vibration (monomer, intermolecular, intramolecular, and polymeric) [30]. The absorption band at 1,637 cm^{-1} due to the presence of O–H bending vibration is probably because of the reabsorption of water from the atmosphere [31].

3.3. Structural characteristics of TiO_2 nanoparticles

The above results indicated that the precursor titanate obtained was in nanostructure, which is further confirmed by TEM observation. The homogeneity, uniformity, and the size of the resulting TiO_2 crystals were studied by TEM, as shown in Fig. 4. TEM study

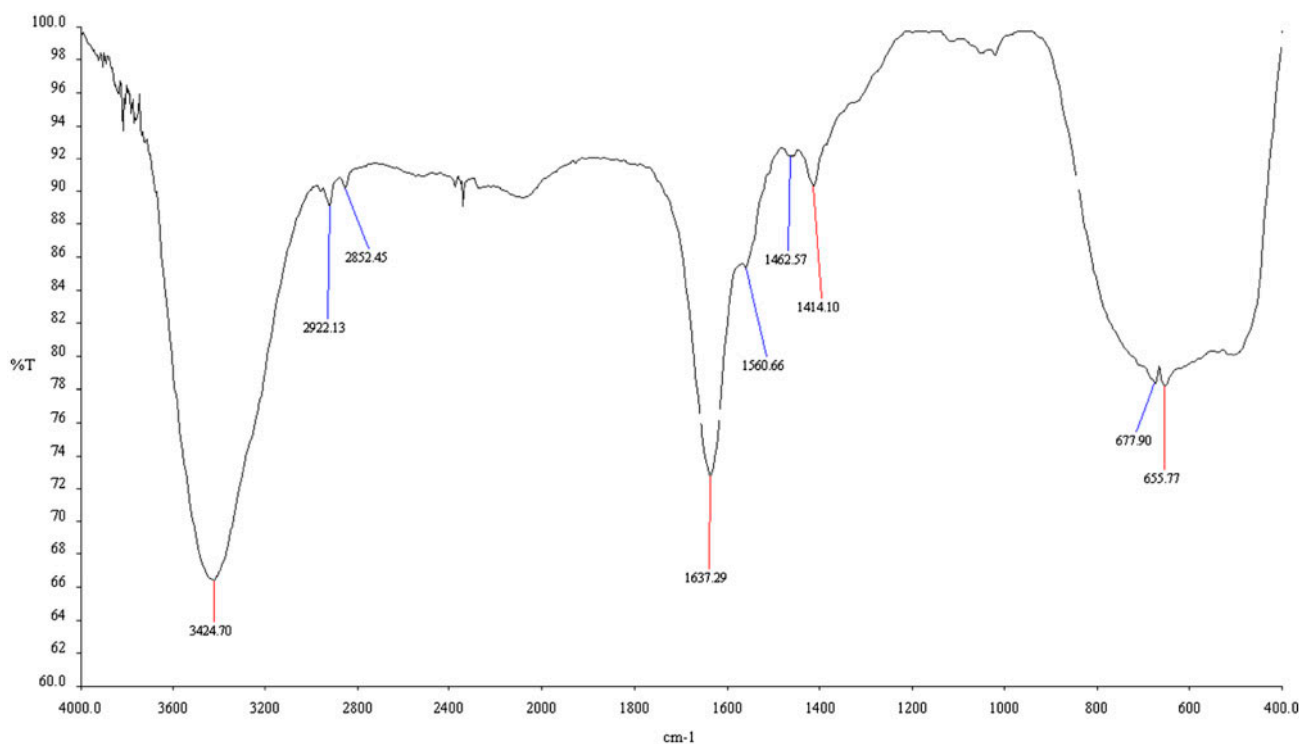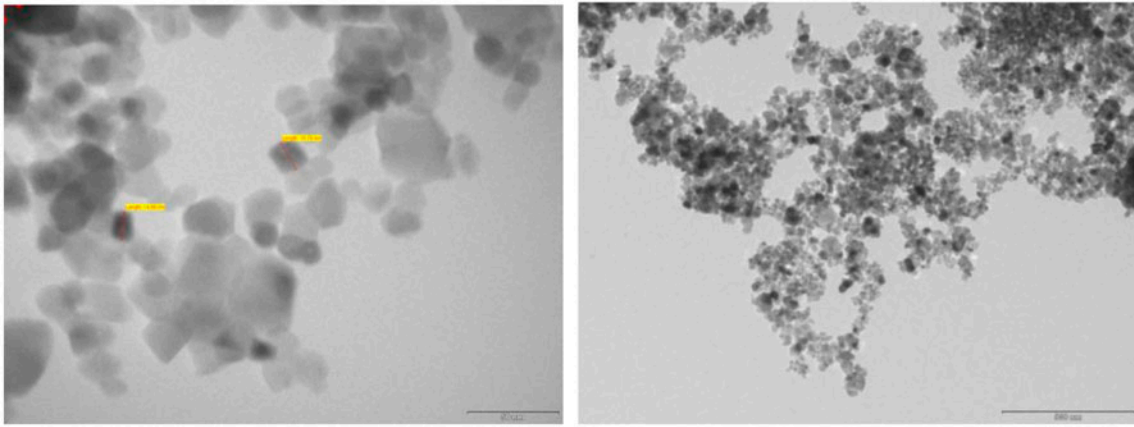Fig. 3. FTIR spectra of synthesized TiO_2.

Fig. 4. TEM image of synthesized TiO$_2$ nanoparticles.

indicated that all the crystals were completely separated from each other and uniform with a particle analytical grade with size of 20–30 nm. These particles do not grow together to form bigger particles even after an extensive period of time. It is worth noting that only a small percentage of the total particles exhibit a diameter size bigger than 30 nm. The crystallites had sets of clearly resolved lattice fringes giving evidence that the TiO$_2$ material was highly crystalline [32].

However, there was a slight discrepancy between the particles sizes determined by XRD analysis and TEM. This could be due to the fact that the effective mass approximation is relatively less correct for small

nanoparticles and statistical effects of spatial confinement also influences the optical properties of nanocrystalline semiconductors [33].

3.4. Photocatalytic activity

The experimental set-up for photocatalytic study comprised of UV light chamber. The UV light source was a 15 W mercury lamp with a wavelength of 365 nm. Different dye concentrations (10, 20, 30, and 40 ppm) were used to determine the effect of catalyst. Fluctuation in pH and temperature during experiment was trifling. In order to evaluate the maximum decolorization
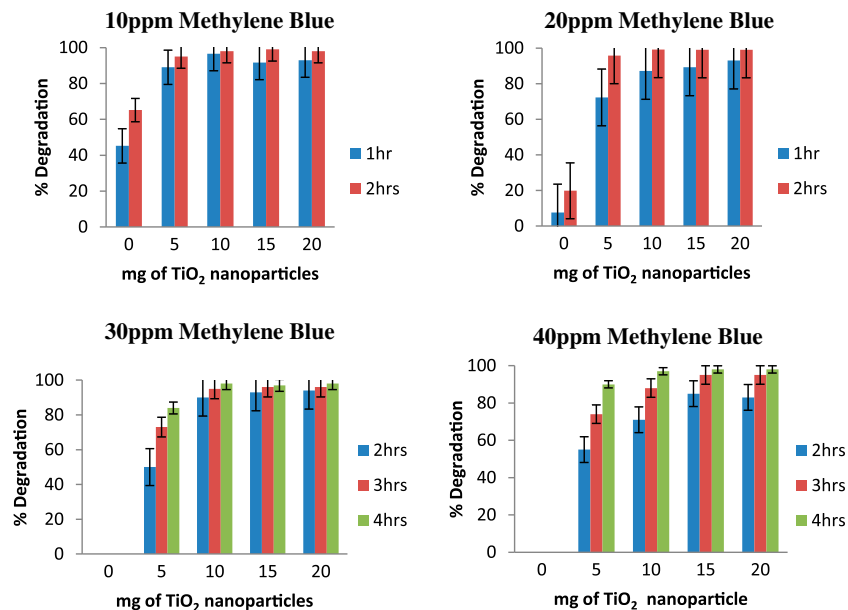

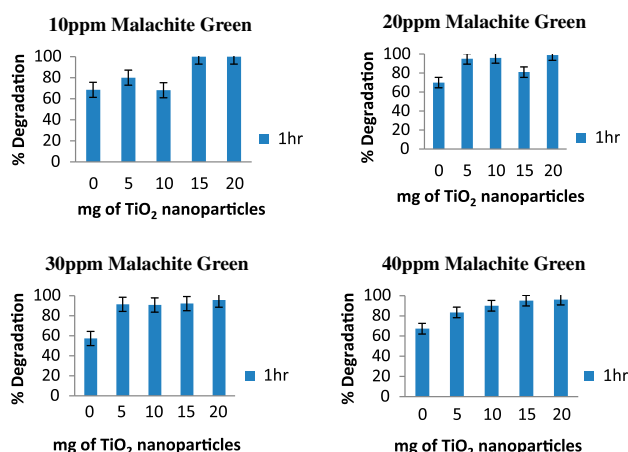Fig. 5. Decolorization of methylene blue by TiO$_2$ nanoparticles.

Fig. 6. Decolorization of malachite green by TiO$_2$ nanoparticles.

capacity of the TiO$_2$ nanoparticles, the effect of catalyst doses-5, 10, 15, and 20 mg was observed. Average result of triplicate experiment has been considered.

3.4.1. Decolorization of methylene blue

The effect of dye concentration on its degradation was studied. Fig. 5 shows the percentage degradation at various methylene dye concentrations. Less concentrated dye (10, 20 ppm) gave complete decolorization at the end of 2 h. Whereas, higher concentrated dye

took almost 4 h for the complete removal of color (Fig. 5). At higher concentration of catalyst, the color removal was found to be high. This may be because as the concentration of the dye increases, the catalyst particles adsorb more and more dye. At higher concentration, the light travels up to a smaller distance.

3.4.2. Decolorization of malachite green

As seen in Fig. 6, malachite green took lesser time by an hour for complete color removal of 10–40 ppm dye. Though figure indicates that dye itself degrades in UV irradiation, the activity was enhanced in presence of catalyst loading.

3.4.3. Decolorization of rhodamine B

Degradation of rhodamine B shown in Fig. 7 clearly demonstrates that the degradation rate increases with the particle dose. However, the removal efficiency was around 96% for 20 mg dose which is five times of the initial value of 20 mg of higher concentrated dye solution. Hence, 20 mg adsorbent can be taken as an optimum dose.

3.4.4. Decolorization of paint industry effluent

It can be seen that there exists a good correlation between the light absorption properties and the photocatalytic activity of the samples. When the particle
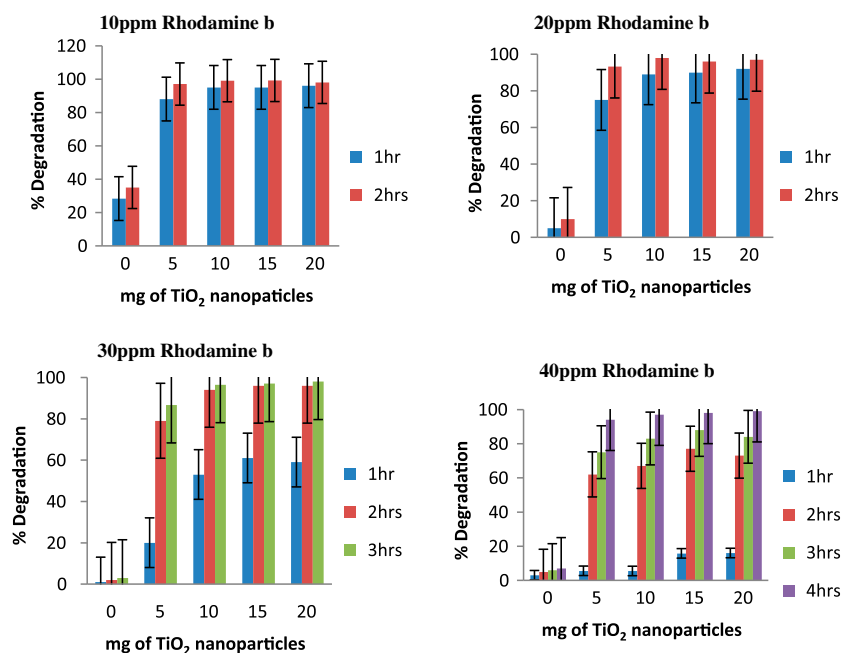

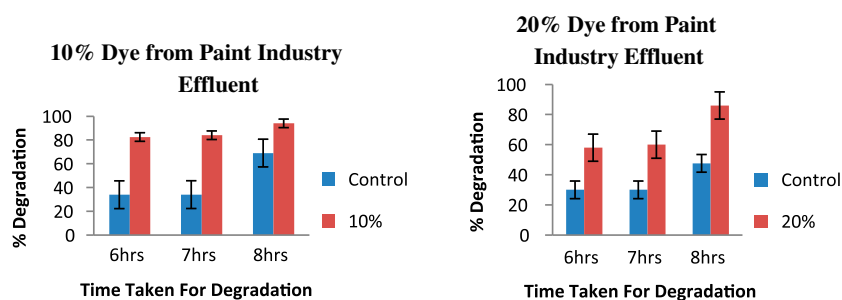Fig. 7. Decolorization of rhodamine B by TiO$_2$ nanoparticles.

10% Dye from Paint Industry Effluent

20% Dye from Paint Industry Effluent

Fig. 8. Decolorization of paint industrial effluent by TiO_2 nanoparticles.

content is 20 mg, photocatalytic activity is significantly improved. Crude effluent took 8 h for 80–95% removal (Fig. 8). Because of the presence of heavy metals, lubricants, oils, and other pollutants in paint industry effluent, degradation took longer time compared to dye solution.

pH, COD, PO_4, SO_4, NO_3, and hardness of the paint industry effluent before photocatalysis was found to be 6, 370, 0.280, 360, 0.198, and 765 mg/L accordingly. On discoloration of effluent, these values changed to 6.8, 360, 0.260, 342, 0.165, and 740 mg/L, respectively.

3.4.5. Decolorization of textile industry effluent

In textile industry effluent, the decoloration efficiency was around 98% which is 5–6 times of the initial value of decoloration. The organic constituent

of diluted wastewater to 10% was almost completely photo oxidized after an irradiation of 3 h (Fig. 9). Effluent was found to be almost completely decolorized on irradiation for 3–5 h. The results showed similar value for adsorption capacity of catalyst for dyes and effluents. At the end of decoloration, physicochemical parameters of textile effluent showed reduction from initial values, like pH value changed to 6.5 from 7.2, COD changed to 389 from 402 mg/L, PO_4 changed to 0.25 from 0.275 mg/L, SO_4 changed to 320 from 340 mg/L, NO_3 changed to 0.155 from 0.175 mg/L, and hardness turned to 500 from 740 mg/L.

Lee et al. suggested that the different percent decoloration can be related to chemical structure, molecular size, and stereo-chemistry of the dyes and effluents [34].
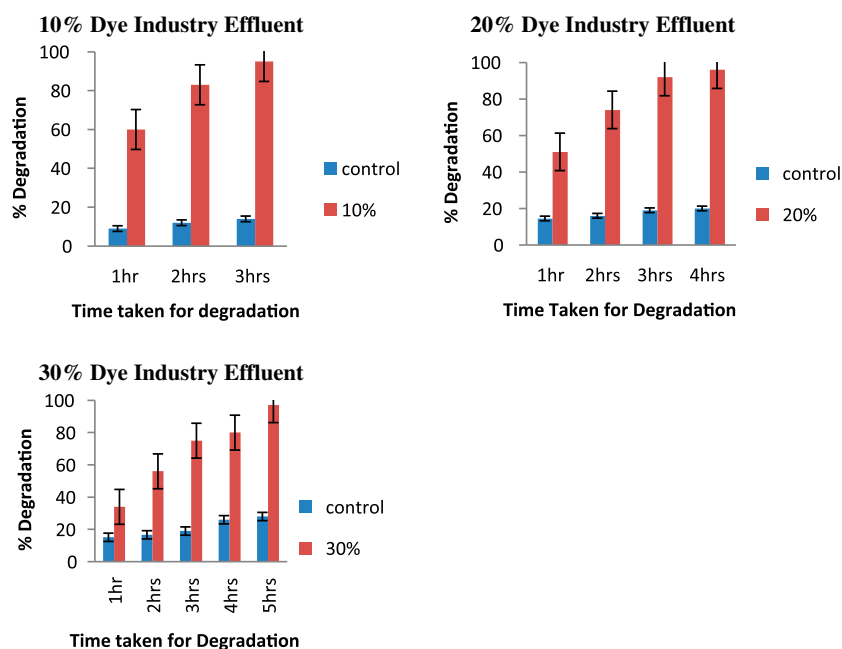
10% Dye Industry Effluent

20% Dye Industry Effluent

30% Dye Industry Effluent

Fig. 9. Decolorization of textile industry effluent by TiO_2 nanoparticles.

4. Conclusion

Crystalline TiO_2 nanoparticles of 20–40 nm were synthesized using sol–gel method and the experiment has revealed that lower acidic conditions promote anatase cuboidal structure. The UV light irradiation of the dye using nanoTiO$_2$ as a catalyst has yielded percentage decoloration greater than 95% for a catalyst loading of 20 mg. The results of the present photocatalytic studies indicate that the maximum degradation of methylene blue and rhodamine B was obtained at 20 mg, 4 h, 40 ppm of catalytic dose, contact time, initial concentration, respectively. On the other hand, the maximum degradation of malachite green was observed at one hour contact time with other similar conditions as in case of methylene blue and rhodamine B dyes. The nano-TiO$_2$ capable of degrading effluents within 3–8 h shows its high affinity and capacity. The developed nanocatalyst system is an efficient and cost-effective method for the removal of the dyes from contaminated water and industrial effluents [35].

References

[1] F. Wurthner, Topics in current chemistry, in: V. Balzani, A. de Meijere, K.N. Houk, H. Kessler, J.-M. Lehn, S.V. Ley, S.L. Schreiber, J. Thiem, B.M. Trost, F. Vögtle, H. Yamamoto (Eds.), Supramolecular Dye Chemistry, Springer-Verlag, New York, NY, 2005, pp. 258–260.

[2] R. Abraham, F.S. Harold, Carbon adsorption of dyes and selected intermediates, encyclopedia of chemical technology, in: Kirk-Othmer (Ed.), Environmental Chemistry of Dyes and Pigments, Wiley, New York, NY, 1996, pp. 672–783.

[3] E.A. Clarke, R. Anliker, Handbook of environmental chemistry, in: O. Hutzinger (Ed.), Organic Dyes and Pigments, Springer-Verlag, Heidelberg, 1980, pp. 181–215.

[4] H. Zollinger, Color Chemistry. Synthesis, Properties and Applications of Organic Dyes and Pigments, VCH, Weinheim, New York, Basel, Cambridge, 1991.

[5] U.G. Akpan, B.H. Hameed, Parameters affecting the photocatalytic degradation of dyes using TiO$_2$-based photocatalysts: A review, J. Hazard. Mater. 170 (2009) 520–529.

[6] N.K. Daud, U.G. Akpa, B.H. Hameed, Decolourization of Sunzol Black DN conc. in aqueous solution by Fenton oxidation process: Effect of system parameters and kinetic study, Desalin. Water Treat. 37 (2012) 1–7.

[7] N. Thinakaran, P. Panneerselvam, P. Baskaralingam, D. Elango, S. Sivanesan, Equilibrium and kinetic studies on the removal of Acid Red 114 from aqueous solutions using activated carbons prepared from seed shells, J. Hazard. Mater. 158 (2008) 142–150.

[8] B.H. Hameed, U.G. Akpan, K.P. Wee, Photocatalytic degradation of Acid Red 1 dye using ZnO catalyst in the presence and absence of silver, Desalin. Water Treat. 27 (2011) 204–209.

[9] W. Baran, E. Admek, A. Makowski, The influence of selected parameters on the photocatalytic degradation of azo-dyes in the presence of TiO$_2$ aqueous suspension, Chem. Eng. J. 145 (2008) 242–248.

[10] K. Lee, N.H. Lee, S.H. Shin, H.G. Lee, S.J. Kima, Hydrothermal synthesis and photocatalytic characterizations of transition metals doped nano TiO$_2$ sols, Mater. Sci. Eng., B 129 (2006) 109–115.

[11] M.T. Sulaka, H.C. Yatmazb, Removal of textile dyes from aqueous solutions with eco-friendly biosorbent, Desalin. Water Treat. 37 (2012) 169–177.

[12] C.R. Chenthamarakshan, K. Rajeshwar, E.J. Wolfrum, Heterogeneous photocatalytic reduction of Cr(VI) in UV-irradiated titania suspensions: Effect of protons, ammonium ions and other interfacial aspects, Langmuir. 16 (2000) 2715–2721.

[13] T. Robinson, G. Mcmullan, R. Marchant, P. Nigam, Remediation of dyes in textile effluent: A critical review on current treatment technologies with a proposed alternative, Bioresour. Technol. 77 (2001) 247–255.

[14] S. Pokharna, R. Shrivastava, Photocatalytic treatment of textile industry effluent using titanium oxide, Int. J. Recent Res. Rev. 2 (2013) 9–17.

[15] R. Reid, Go green—A sound business decision, J. Soc. Dyers Colour. 112 (1996) 103–109.

[16] T.A. Khan, I. Ali, V.V. Singh, S. Sharma, Utilization of fly ash as low-cost adsorbent for the removal of Methylene Blue, Malachite Green, Rhodamine B from textile wastewater, J. Environ. Prot. Sci. 3 (2009) 11–22.

[17] H. Lachheb, E. Puzenat, A. Houas, M. Ksibi, Photocatalytic degradation of various types of dyes in water by UV-irradiated titania, Appl. Catal., B 39 (2002) 75–90.

[18] J. Lee, W. Nam, M. Kang, K. Yoon, M. Kim, K. Ogino, S. Miyata, S. Choung, Design of two types of fluidized photo reactors and their photo-catalytic performances for degradation of methyl orange, Appl. Catal., A 244 (2003) 49–57.

[19] R.J. Tayadea, P.K. Suroliaa, R.G. Kulkarnib, R.V. Jasraa, Photocatlytic degradation of dyes and organic contaminants in water using nanocrystalline anatase and rutile TiO$_2$, Sci. Technol. Adv. Mater. 8 (2007) 455–462.

[20] B.D. Cam, N. Thi, D. Cam, P.T. Dong, D.T. Phuong, Silver doped titania materials on clay support for enhanced visible light photocatalysis, e-J. Surf. Sci. Nanotechnol. 9 (2011) 454–457.

[21] C. Suresh, V. Biju, P. Mukundan, K.G.K. Warrier, Anatase to rutile transformation in sol–gel titania by modification of precursor, Polyhedron 17 (1998) 3131–3135.

[22] Y.F. Chen, C.Y. Lee, M.Y. Yeng, H.T. Chiu, The effect of calcination temperature on the crystallinity of TiO$_2$ nanopowders, J. Cryst. Growth 247 (2003) 363–370.

[23] S. Kathirvelu, L. D'Souza, B. Dhurai, UV protection finishing of textiles using ZnO nanoparticles, Indian J. Fibre Text. Res. 34 (2009) 267–273.

[24] M. Pelaez, A. Cruz, E. Stathatos, P. Falaras, D.D. Dionysiou, Visible light-activated N-F-codoped TiO$_2$ nanoparticles for the photocatalytic degradation of microcystin-LR in water, Catal. Today 144 (2009) 19–25.

[25] J.P. Nikkanen, T. Kanerva, T. Mantyla, The effect of acidity in low-temperature synthesis of titanium dioxide, J. Cryst. Growth 304 (2007) 179–183.

[26] H. Cheng, M. Jiming, Z. Zhenguo, Q. Limin, Hydrothermal preparation of uniform nanosize rutile and anatase particles, Chem. Mater. 7 (1995) 663–671.

[27] C. Sanchez, J. Livage, M. Henry, F. Babonneau, Chemical modification of alkoxide precursors, J. Non-Cryst. Solids 100 (1988) 65–76.

[28] H.S. Jung, K.S. Hong, J.K. Lee, Crystallization process of TiO$_2$ nanoparticles in an acidic solution, Chem. Lett. 33 (2004) 1382–1383.

[29] N. Phonthammachai, T. Chairassameewong, E. Gulari, A.M. Jamieson, S. Wongkasemjit, Structural and rheological aspect of mesoporous nanocrystalline TiO$_2$ synthesized via sol–gel process, Microporous Mesoporous Mater. 166 (2003) 261–271.

[30] H. Choi, E. Stathatos, D. Dionysiou, Sol–gel preparation of mesoporous photocatalytic TiO$_2$ films and TiO$_2$/Al$_2$O$_3$ composite membranes for environmental applications, Appl. Catal., B 63 (2006) 60–67.

[31] S.V. Gaponenko, Optical Properties of Semiconductor Nanocrystals, Cambridge University Press, Cambridge, 1998.

[32] J. Mohan, in: A. Nilchi (Ed.), Organic Spectroscopy Principles and Applications, Narosha Publishing House Pvt. Ltd., New Delhi, 2009, pp, 28–95.

[33] R.A. Aziz, I. Sopyan, Synthesis of TiO$_2$–SiO$_2$ powder and thin film photocatalysts of sol–gel method, Int. J. Chem. 48 (2009) 951–957.

[34] J.W. Lee, W.G. Shim, W.C. Yang, H. Moon, Adsorption equilibrium of amino acids and antibiotics on non-ionic polymeric sorbents, J. Chem. Technol. Biotechnol. 79 (2004) 413–420.

[35] W. Au, S. Parhak, C.J. Collie, T.C. Hsu, Cytogenetic toxicity of gentian violet and crystal violet on mammalian cells *in vitro*, Mutat. Res. 58 (1978) 269–276.